Superlattice Assembly by Interpolymer Complexation: Supporting Information

Nathan Horst,[†] Srikanth Nayak,[‡] Wenjie Wang,[¶] Surya Mallapragada,[‡,†] David Vaknin,[§] and Alex Travesset[*,†,§]

†*Ames Laboratory, and Department of Materials Science and Engineering*

‡*Ames Laboratory, and Department of Chemical and Biological Engineering*

¶*Division of Materials Science and Engineering, Ames Laboratory, USDOE, Ames, Iowa 50011, United States*

§*Ames Laboratory, and Department of Physics and Astronomy, Iowa State University, Ames, Iowa 50011, United States*

E-mail: trvsst@ameslab.gov

Effect of PAA length on IPC-mediated assemblies

In our study, Figure 2 shows the structure factor curves obtained for nanoparticle assemblies with varying PAA lengths. With PAA100kDa, the structure factor ($S(Q)$) shows a broad primary peak at $Q_0 = 0.023\text{Å}^{-1}$ indicating a characteristic inter-particle distance of $\frac{2\pi}{Q_0} \simeq 273$Å. Broadness of the peak indicates poor crystallinity/packing in the assemblies. In fact, the assemblies are visible as floating agglomerates of nanoparticles in the suspension and not as precipitates. In the case of both PAA2k and PAA5k, visible precipitates form in the vials. The structure factor shows features characteristic of the FCC symmetry, which is in agreement with our previous findings.[2] For both PAA2k and PAA5k, the inter-particle distance is $\frac{\sqrt{6}\pi}{Q_0} \simeq 257$ Å, and $\simeq 265$ Årespectively. In the case of assemblies obtained with

propionic acid, there are agglomerates of nanoparticles, and the corresponding inter-particle distance in the assemblies is $\simeq 453$ Å. These results are tabulated in Table S1.

Table S1: Summary of SAXS results for IPC-mediated nanoparticle assemblies obtained with varying lengths of PAA. Q_0 is the primary peak position in the structure factor curves, and D_n is the inter-particle distance in the assemblies

PAA	# monomers	Q_0 (Å^{-1})	D_n (Å)
Propionic acid	1	0.017	453
2k	28	0.030	257
5k	69	0.029	265
100k	1389	0.023	273*

Results show that the molecular weight of PAA, under the same monomer concentration, has an effect on the structure of the nanoparticle assemblies formed via IPCs. Particularly, very large molecular weight PAA chains (100kDa) lead to poor crystallinity. It is hypothesized that higher molecular weight polymers form IPCs more readily compared to lower molecular weight polymers, due to the cooperative effect.[3,4] In fact, a lower limit to the molecular weight of the polymer required to form IPCs is shown.[5,6] We have shown that even PEG with molecular weight as low as 800Da can lead to IPC-mediated assembly with PAA2kDa.[2] This is likely due to the grafted nature of the PEG. The high local density of PEG chains could effectively act as a higher molecular weight system. Here, we show that even propionic acid can lead to nanoparticle assembly. Higher inter-particle distance shows that these assemblies are more hydrated compared to those obtained with PAA2k and PAA5k. Interestingly, propionic acid cannot directly bridge two nanoparticles, unlike PAA chains. However, this does not seem to prevent the formation of the assemblies. This may indicate the presence of solvent mediated effects and Van Der Waals forces in assembly formation and stability.

Theta Temperature

We determine the P_A θ-temperature T_θ, by examining the radius of gyration for differing P_A lengths and temperatures as shown in Fig. S1.

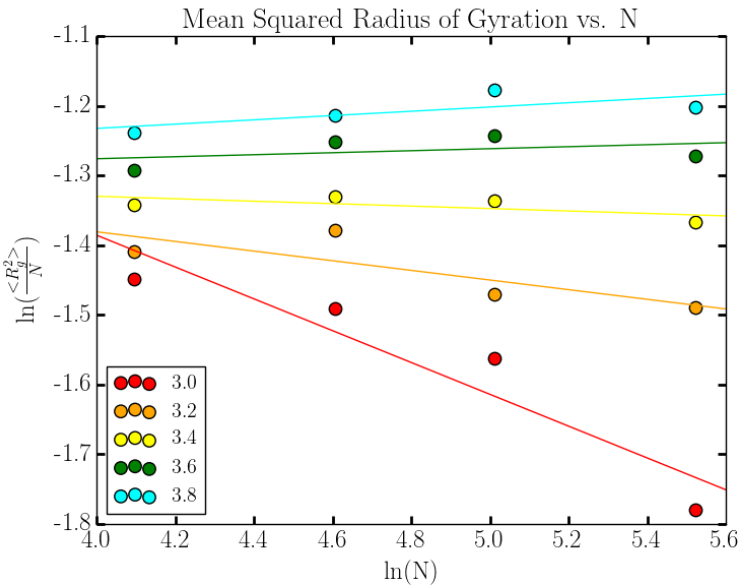

Figure S1: The theta temperature of our polymer corresponds to T = 3.5, where $\log(\frac{<R_g^2>}{N})$ is constant for increasing $\log(N)$.

Hybridizations

The nature of our non-bonded hybridization potential allows for "proximity hybridizations" as illustrated in Fig. S3. We find that multiple hybridizations can occur at the same site, but clearly, these hybridizations would vary in strength. The choice of $1.5\sigma_H$ as the definition of a hybridization event ensures that two beads directly opposite a central complementary bead cannot both simultaneously hybridize, regardless of hybridizer orientation. We note that the CG beads that we use represent many monomer groups of the real system, but we acknowledge that precise understanding of the necessary number of hydrogen bonds to drive IPC would require a model with more specificity.

Hybridization lifetimes are determined for each logged timestep when a given pair of hybridizers are within hybridization distance. Once the hybridization dissociates, we terminate the lifetime between those hybridizers, which ensures that if there is no exchange outside the local area, recombination is not counted towards the average hybridization lifetime. This approach does not account for the lifetime of a hybridization accomplished through multiple hybridizers, but due to the excess of exchange in the corona, and our counting criteria, we are confident that the lifetimes presented are typical of the system.

To calculate hybridization residency time within the P_A corona, we determine how many of the P_D beads that reside in the P_A corona are exchanged with the bulk material surrounding an isolated NC. We see that the flux of P_D beads in and out of the corona is large at high ξ, and tends towards zero as ξ is lowered (Fig. 8b). P_D is completely absorbed into the corona when ξ is sufficiently low, leading to a net zero flux out of the corona. However, when we split the corona into two separate shells of equal width (inner and outer), and determine the flux of P_D in and out of these shells; where, at a net zero flux out of the corona, P_D is clearly still exchanged (Fig. 8b). Our analysis of hybridization lifetimes and residency times gives us confidence that we avoid quenching and witness equilibrium behavior in our simulations.

OPM Model

The optimal packing model (OPM)[1] defines a dimensionless nearest neighbor distance between two NCs as

$$\tau_{OPM} = (1 + 3\nu\lambda)^{1/3} \tag{1}$$

where

$$\lambda = \frac{L}{R_c} \tag{2}$$

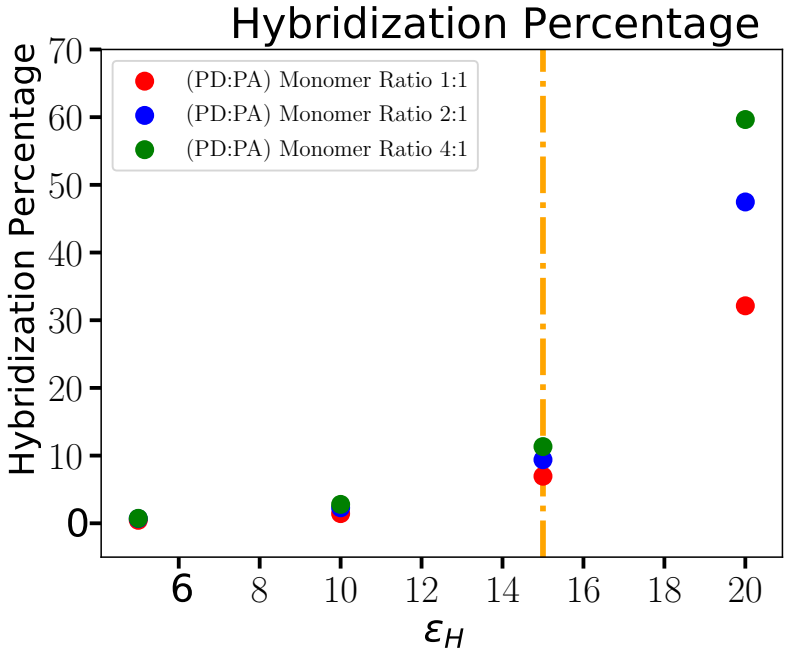

Figure S2: Percentage of hybridized particles in the P_D/P_A melt. The orange dotted line corresponds to the value at $\epsilon_H = 15$, where hybridizations are happening more readily, but stoichiometry plays less of a role.

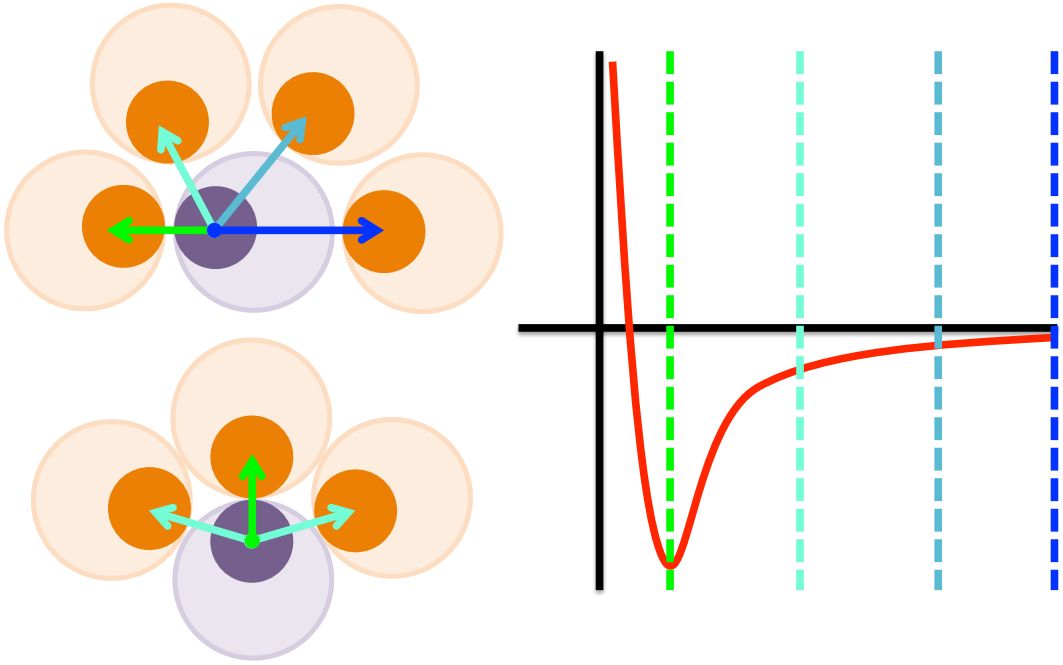

Figure S3: Examples of how the hybridization model can lead to configurations where multiple "proximity hybridizations" are formed at the same site for a generic short-ranged interaction potential.

is the dimensionless contour length of the grafted polymer, with NC core radius R_c and L the contour length of the grafted polymer chain, and

$$\nu = \frac{A_0}{A_i} \tag{3}$$

with A_i is the molecular area of the bound polymer to the core surface, and A_0 the cross section of the bound polymer, which leads to a dimensionless grafting density defined by $\frac{1}{\nu}$ which for densely grafted systems is $\frac{1}{\nu} \simeq 1$. Our calculations for experimental systems use $L = (2l_{co} + l_{cc})\cos(\theta/2)N_r = 3.64N_r$ for PEG, with N_r equal to the number of C-O-O groups along the chain, $l_{co} = 1.43$ and $l_{cc} = 1.53$ the C-O and C-C bond lengths, and $\theta = 68°$ the bond angle. We do not include PAA in the calculation of contour length, and we assume maximum grafting density in our system, with $\nu = 1$. The calculations for our CG model are straightforward, as the particles are built with maximum grafting density, N_r is equal to the number of CG beads in the P_A chain and $L = 0.84N_r$, commensurate with the CG bond length of 0.84.

Lattice Bridges

Characterizing BE in the lattice requires that we take advantage of lattice symmetry, in order to obtain statistically relevant information. We can collect all the BE into a single symmetric point for our lattice, by the method shown in Fig. S4, leading to the analysis in Figures S5 to S11. These analysis methods show clearly consistent configurational behavior regardless of ξ.

References

(1) Landman, U.; Luedtke, W.D., Small is different: energetic, structural, thermal and mechanical properties of passibated nanocluster assemblies. *Faraday Discuss.* **2004**, *125*,

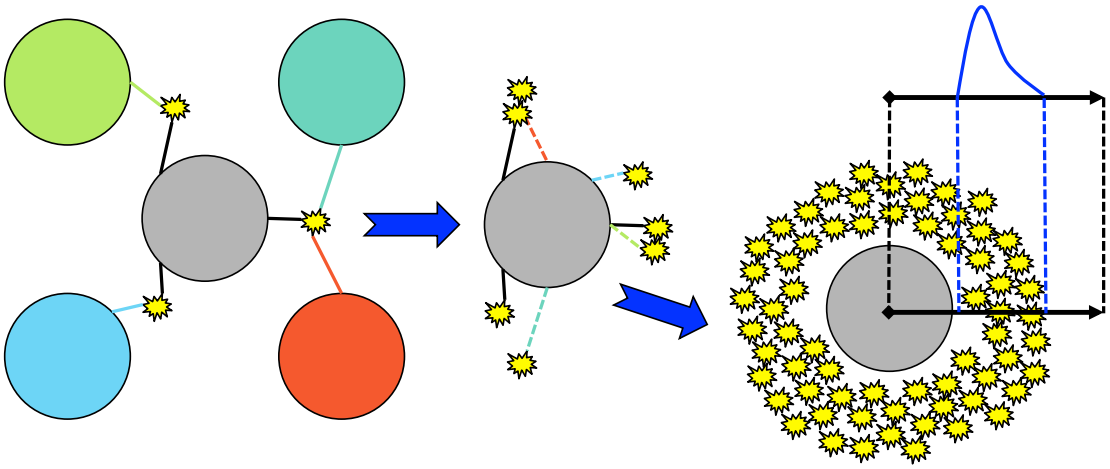

Figure S4: Schematic showing the general process by which bridging events were projected via lattice symmetry into a single NC representation. These projections allow for statistically relevant slices along lines of interest.

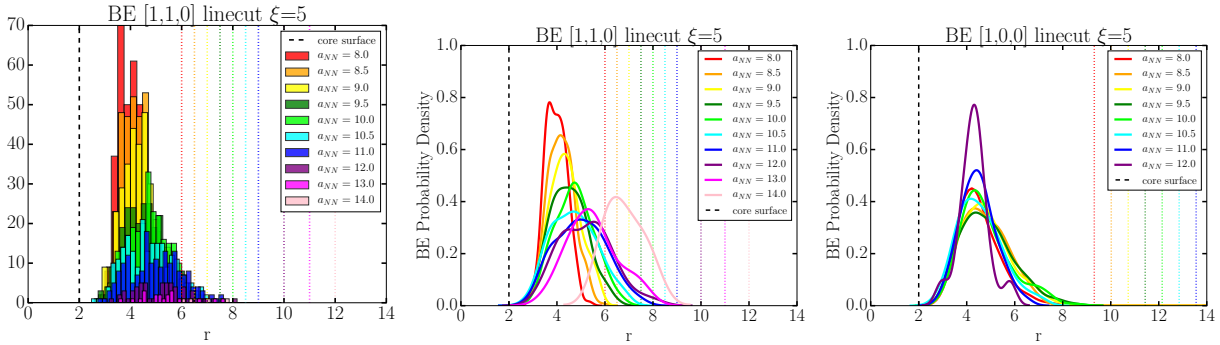

Figure S5: Collection of bridging events for various a_{NN}, and probability densities of bridging events along NN and 2NN lines in the fcc lattice, $\xi = 5$. The leftmost image reinforces the level of statistics present when calculating locational probability densities, where in some cases at large a_{NN}, non-gaussian behavior is due to low statistics.

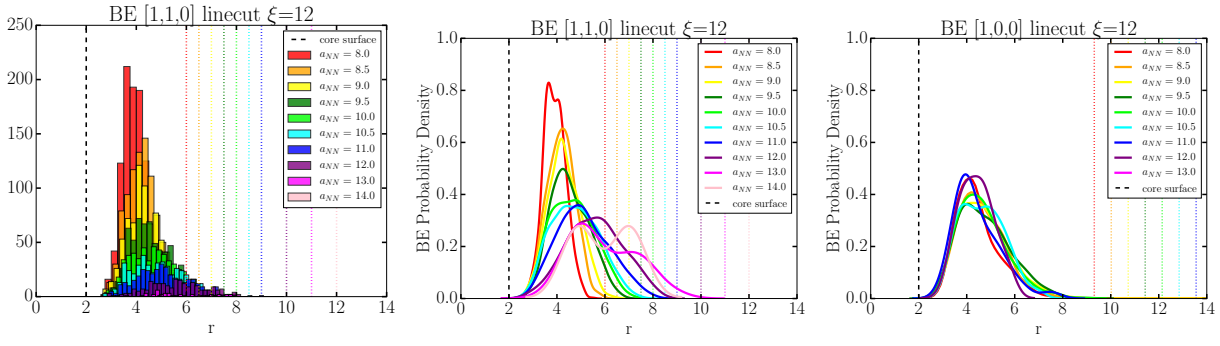

Figure S6: Collection of bridging events for various a_{NN}, and probability densities of bridging events along NN and 2NN lines in the fcc lattice, $\xi = 12$. The leftmost image reinforces the level of statistics present when calculating locational probability densities, where in some cases at large a_{NN}, non-gaussian behavior is due to low statistics.

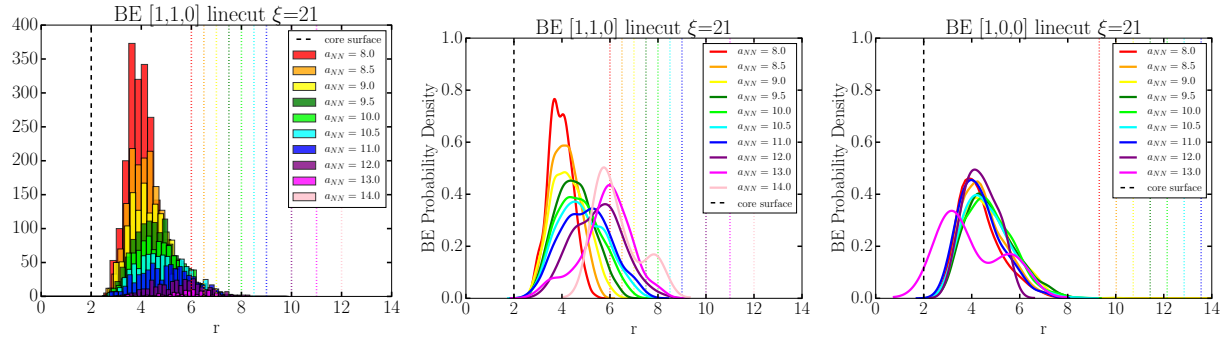

Figure S7: Collection of bridging events for various a_{NN}, and probability densities of bridging events along NN and 2NN lines in the fcc lattice, $\xi = 21$. The leftmost image reinforces the level of statistics present when calculating locational probability densities, where in some cases at large a_{NN}, non-gaussian behavior is due to low statistics.

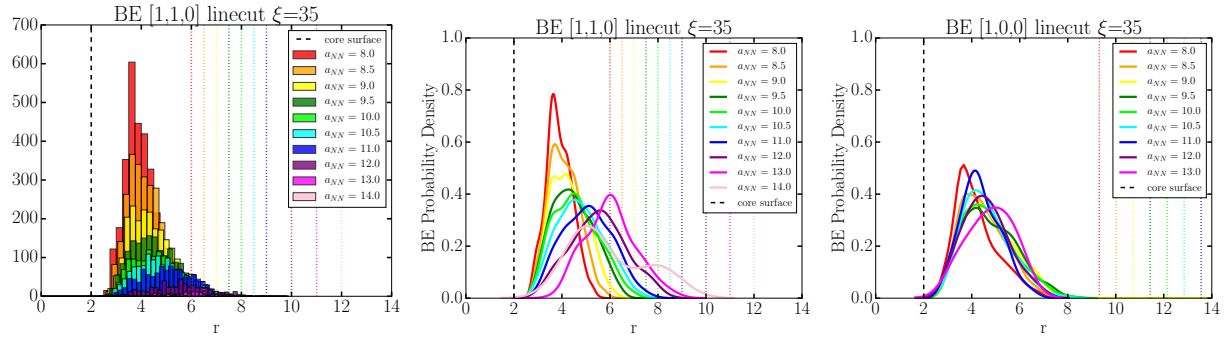

Figure S8: Collection of bridging events for various a_{NN}, and probability densities of bridging events along NN and 2NN lines in the fcc lattice, $\xi = 35$. The leftmost image reinforces the level of statistics present when calculating locational probability densities, where in some cases at large a_{NN}, non-gaussian behavior is due to low statistics.

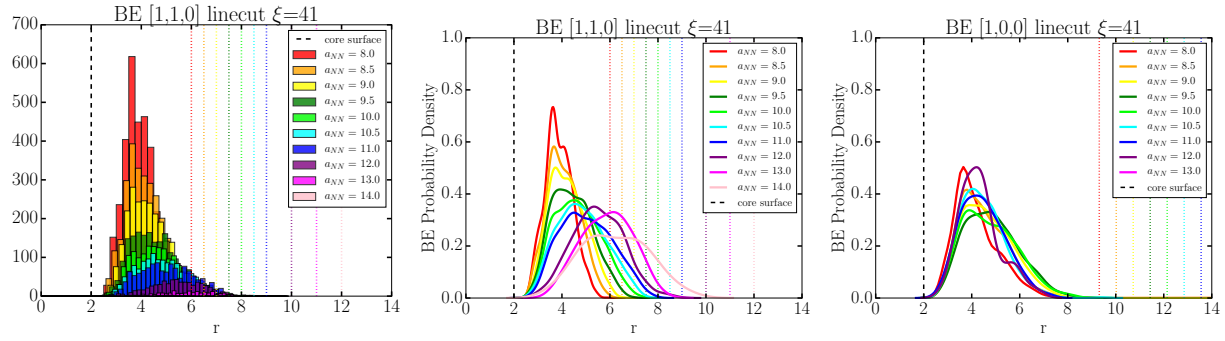

Figure S9: Collection of bridging events for various a_{NN}, and probability densities of bridging events along NN and 2NN lines in the fcc lattice, $\xi = 41$. The leftmost image reinforces the level of statistics present when calculating locational probability densities, where in some cases at large a_{NN}, non-gaussian behavior is due to low statistics.

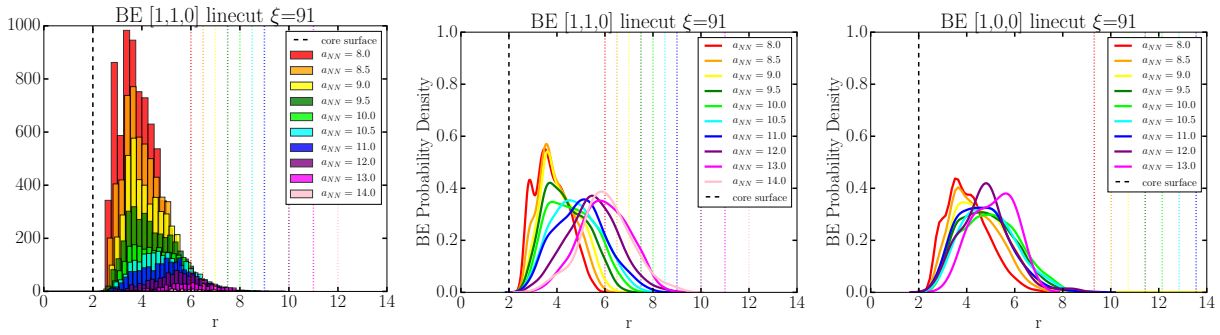

Figure S10: Collection of bridging events for various a_{NN}, and probability densities of bridging events along NN and 2NN lines in the fcc lattice, $\xi = 91$. The leftmost image reinforces the level of statistics present when calculating locational probability densities, where in some cases at large a_{NN}, non-gaussian behavior is due to low statistics.

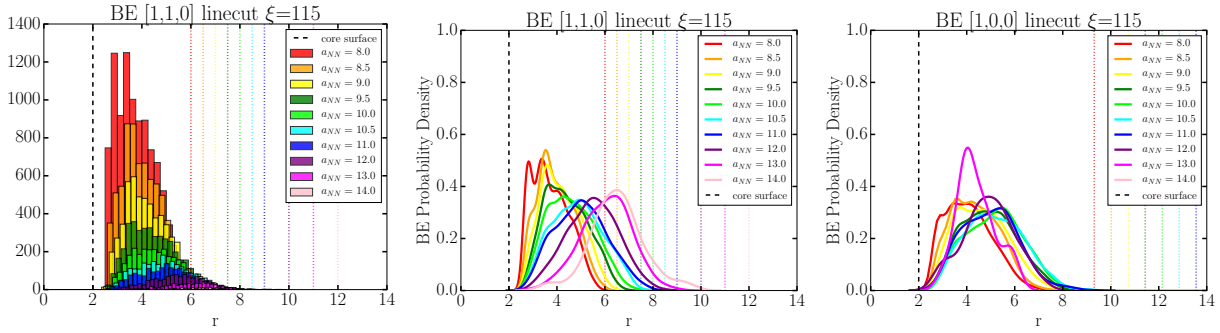

Figure S11: Collection of bridging events for various a_{NN}, and probability densities of bridging events along NN and 2NN lines in the fcc lattice, $\xi = 115$. The leftmost image reinforces the level of statistics present when calculating locational probability densities, where in some cases at large a_{NN}, non-gaussian behavior is due to low statistics.

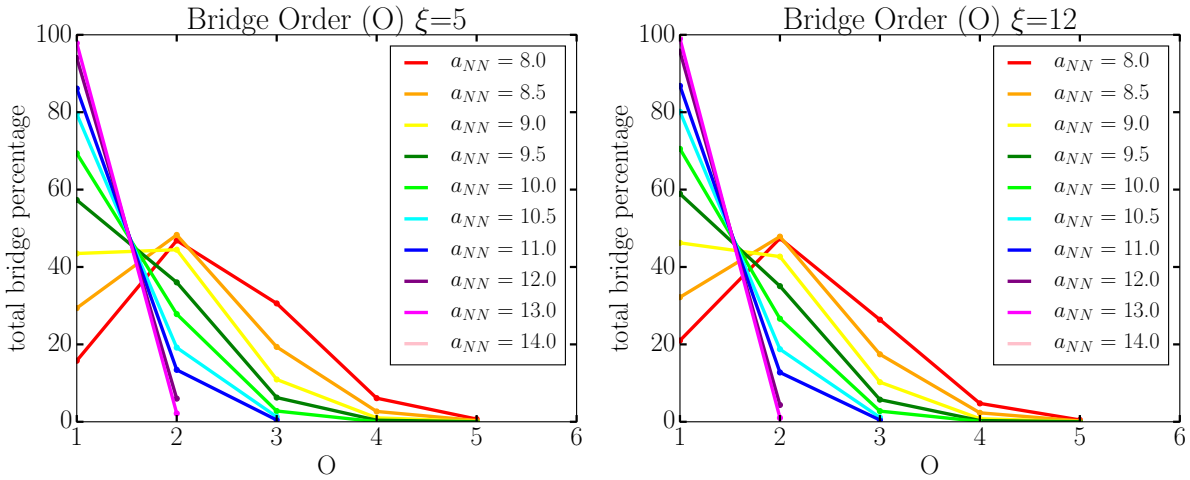

Figure S12: These plots show the bridge order (O) for given values of ξ.

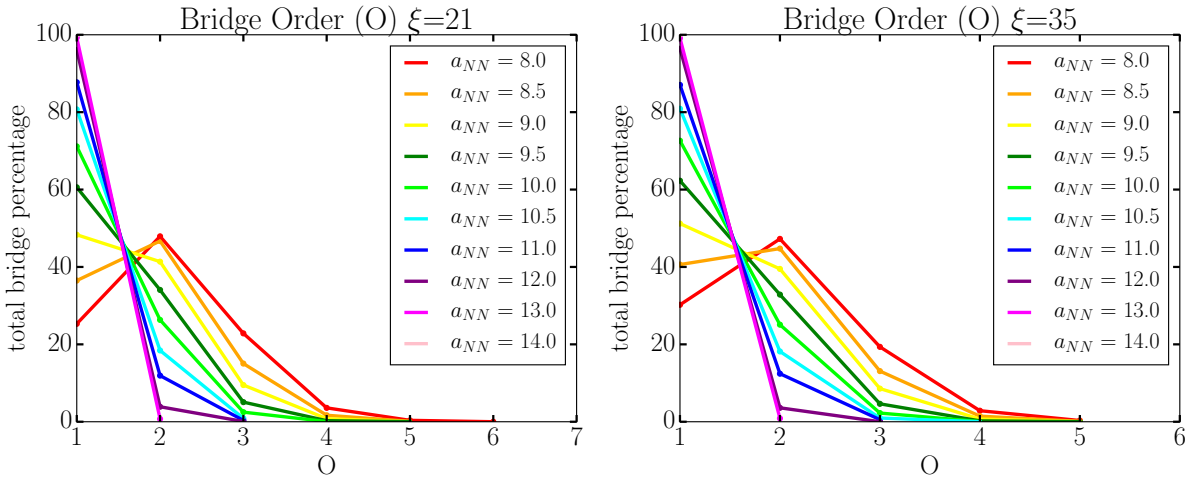

Figure S13: These plots show the bridge order (O) for given values of ξ.

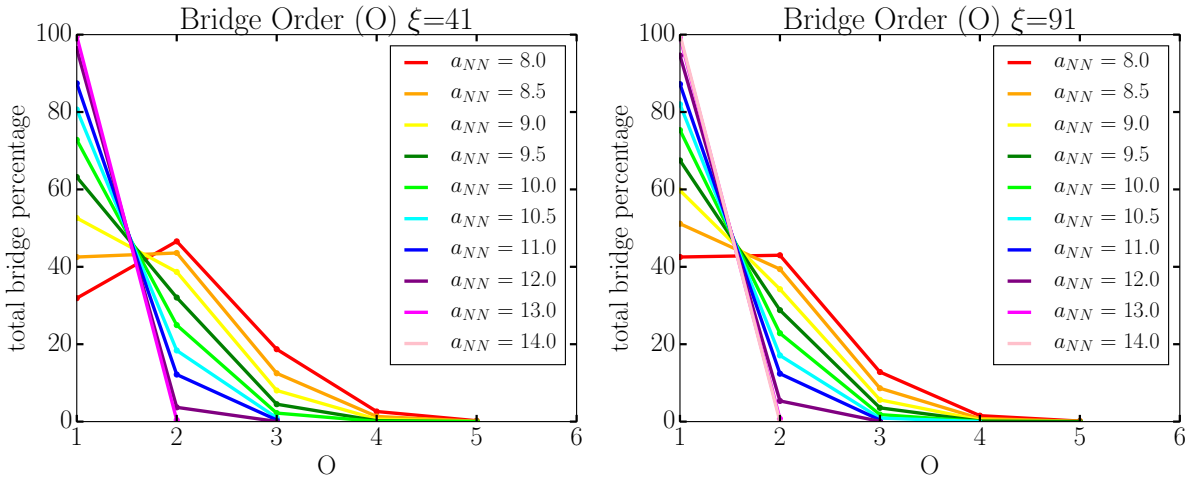

Figure S14: These plots show the bridge order (O) for given values of ξ.

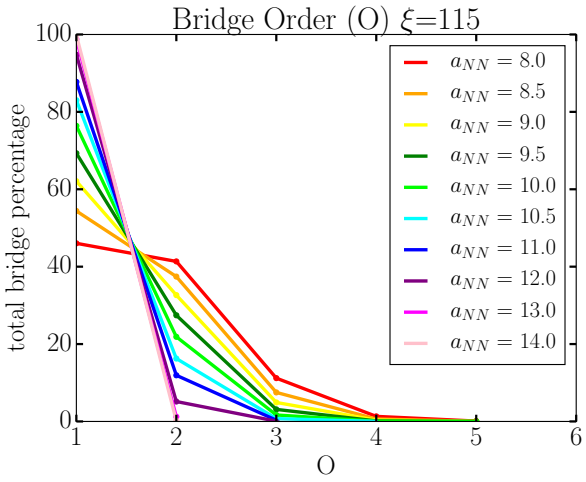

Figure S15: These plots show the bridge order (O) for $\xi = 115$.

1-22.

(2) Nayak, S.; Horst, N.; Zhang, H.; Wang, W.; Mallapragada, S.;Travesset, A.; Vaknin, D. Interpolymer Complexation as a Strategy for Nanoparticle Assembly and Crystallization. *The Journal of Physical Chemistry C* **2019**, *123*, 836-840.

(3) Pradip; Maltesh, C.; Somasundaran, P.; Kulkarni, R.; Gundiah, S. Polymer-polymer complexation in dilute aqueous solutions - poly(acrylic acid)-poly(ethylene oxide) and poly(acrylic acid)-poly(vinyl pyrolidone). *Langmuir* **1991**, *7*, 2108-2111;.

(4) Hao, J.; Yuan, G.; He, W.; Cheng, H.; Han, C.; Wu, C. Interchain hydrogen-bonding-induced association of poly(acrylic acid)-graft-poly(ethylene oxide) in water. *Macromolecules* **2010**, *43*, 2002-2008.

(5) Antipina, A. D.; Baranovskii, V. Y.; Papisov, I. M.; Kabanov, V. A. Equilibrium peculiarities in the complexing of polymeric acids with poly (ethylene glycols). *Polymer Science U.S.S.R.* **1972**, *14*, 1047-1057.

(6) Kabanov, V. A.; Papisov, I. M. Formation of complexes between the complementary synthetic polymers and oligomers in dilute solutions. *Vysokomolekulyarnye Soedineniya Seriya A* **1979**, *21*, 243-281.